CrossMark

ORIGINAL PAPER

Different characteristics of the quasi-biweekly oscillation over the South China Sea in two boreal summer stages

Xu Wang[1] · Guanghua Chen[1] · Ronghui Huang[1]

Abstract This study investigates different evolutions and spatial structures of the quasi-biweekly oscillation (QBWO) over the South China Sea (SCS) during the early (May–June, MJ) and late (August–September, AS) summers of 1991–2010. During the MJ stage, a local QBWO in convection is dominant over the SCS, which is strengthened by the southwestward extension of QBWO anomaly from the east of Japan. In contrast, the QBWO during the AS stage originates from the east of the Philippines and propagates northwestward and then westward until attaining maturation over the SCS, followed by a gradual decay while moving westward. Regarding the circulations, the QBWO during the MJ stage is accompanied by a wave train of lower-level circulation anomalies extending from the SCS to the North Pacific. However, it is found that a wave train exists from the equator to the north of the SCS during the AS stage. In the vertical structures, the QBWO exhibits a northeast tilted relative vorticity with height during the MJ stage, while a vorticity anomaly extending from the surface up to near 300 hPa, but with an opposite above during the AS stage. In general, the QBWO active phases during both stages are characterized by the low-level convergence and cold anomaly and upper-level divergence and warm anomaly, with a strong upward motion. However, the cold anomaly at the low level is prominent during the MJ stage in contrast to that during the AS stage. And the warm anomaly at the upper level reveals a distinct enhancement from the MJ to AS stage.

1 Introduction

The quasi-biweekly oscillation (QBWO) is one of the most important components of the tropical interaseasonal oscillation (ISO), whose time scale is between the synoptic and the Madden-Julian oscillation (MJO; Madden and Julian 1971, 1972) scales. The QBWO signal was found in the power spectra of the meridional wind over the Indian region during the 1967 monsoon season (Keshavamurty 1971). Characteristics about this quasi-biweekly monsoon disturbance were as follows: a 15–20-day period, from sea level to 400 hPa, most marked at 850 hPa, with a wavelength of 34° (longitude) and a phase velocity of 1.7° (longitude) per day from east to west. Moreover, this disturbance was associated with Indian monsoon depression (Keshavamurty 1972). More previous studies reported predominant QBWO signals over the Indian Ocean and western Pacific regions in precipitation and wind through spectral analyses (Murakami and Frydrych 1974; Zangvil 1975; Krishnamurti and Bhalme 1976; Murakami 1976; Krishnamurti and Ardanuy 1980; Chen and Chen 1993; Kiladis and Wheeler 1995; Numaguti 1995). Besides, pronounced QBWO signals were also found in outgoing long wave radiation (OLR) and vorticity fields (Fukutomi and Yasunari 1999; Chen and Sui 2010), and other fields.

MJO, as a key component of ISO, has been studied in a great deal of research (Zhou and Miller 2005; Li et al. 2009; Li and Zhou 2014; Ling et al. 2014). However, characteristics of QBWO, which is also a part of ISO in the tropics, draw more and more attentions in recent years, because of its strong impacts on important weather and climate systems in both

✉ Guanghua Chen
cgh@mail.iap.ac.cn

[1] Center for Monsoon System Research, Institute of Atmospheric Physics, Chinese Academy of Sciences, P.O. Box 2718, Beijing 100190, China

tropical and subtropical regions. Kikuchi and Wang (2009) reviewed that the QBWO was quite significant in boreal summer, and there were mainly three active regions: the Asia-Pacific, the Central America, and the South Pacific regions. The QBWO had a connection with monsoon circulations during the summer, and its activities were complicated and diverse in these regions. However, QBWO could be briefly classified into westward propagating modes associated with equatorial Rossby waves and eastward propagating modes connected with upstream extratropical Rossby wave trains. In other ways, it was documented that the QBWO could influence the active/broken cycles of Indian summer monsoon (Krishnamurti and Ardanuy 1980; Yasunari 1981; Goswami et al. 2003) and South China Sea (SCS) summer monsoon (Chen et al. 2000; Chan et al. 2002; Mao and Chan 2005; Zhou and Miller 2005). Some studies also indicated that the QBWO was closely related to the rainfall in the Yangtze and Huai River basin of China in boreal summer (Yang et al. 2010; Liu et al. 2014). Besides, the QBWO could impact the track of the tropical cyclone. Some research indicates a typhoon that originally propagated westward might turn northward when it encountered a QBWO disturbance (Liang et al. 2011; Wu et al. 2011).

Previous studies mainly focused on the seasonal characteristics of the QBWO but paid less attention to its intraseasonal variation. Kemball-Cook and Wang (2001) found that the life cycle of ISO (10–100 days) in the tropics in early boreal summer was different from that in late summer. They divided the boreal summer into two periods, i.e., May–June (MJ, the early summer) and August–October (ASO, the late summer) periods, and they found that the climatological propagation characteristics of the convective anomalies at the ISO scale from the Indian Ocean to the western Pacific are quite different in MJ and ASO. The convection in MJ showed a strong eastward propagation along the equator, while that in ASO was associated with a weaker eastward-moving signal along the equator and a discontinuous jump from the Indian Ocean to the western Pacific. In marked contrast to the MJ life cycle, the ASO life cycle showed a strong northwestward propagation of convection in the western Pacific. Besides, Wang et al. (2009) divided boreal summer into early summer (May–June) and late summer (July–August) to investigate distinct principal modes of rainfall anomalies in East Asia (EA). In their study, remarkable differences in mean state and the principal modes of interannual precipitation variability were exhibited during the early and late summer. Later, Yang et al. (2014) demonstrated the differences of quasi-biweekly characteristics over EA at early and late summer. However, SCS, as a part of the Asia-Pacific, is also a crucial region for QBWO. Does the QBWO over SCS also have distinct characteristics in different stages of boreal summer? We will address this issue in this paper.

The paper is organized as follows. Section 2 describes the data and methodology used in this study. In Section 3, variance distributions of the QBWO in two summer stages are given, and power spectral analysis is conducted to check the QBWO signals. The different space–time evolutions of the QBWO and their corresponding low-level circulations during the early and late stages are presented in Section 4. In Section 5, the vertical structures associated with the QBWO during the two stages are compared. A preliminary analysis and discussion are presented to interpret the differences of QBWO characteristics in both stages in Section 6. Finally, the results are summarized in Section 7.

2 Methodology

In this study, OLR was used as a proxy of deep tropical convection, as in Liebmann (1996). The daily OLR data covered the period of 1 May to 30 September from 1991 to 2010 on a $2.5° \times 2.5°$ grid. The daily meteorological fields were derived from the National Centers for Environmental Prediction-National Center for Atmospheric Research (NCEP-NCAR) reanalysis project (Kalnay et al. 1996), with the same period and the same grid as the OLR. Prior to filtering, the liner trend and the annual cycle based on 20-year daily data were removed from the time series.

Lanczos filtering (Duchon 1979) was applied to extract the QBWO signals from the OLR and circulation fields based on a 10–20-day filtering window. For a 10–20-day oscillation, a Lanczos digital filter with 53 daily weight coefficients would provide a sharp cutoff response with negligible Gibbs oscillation. Fifty-three was the minimum total number of weights required to achieve unit response at the band center (Duchon 1979; Chen and Sui 2010). Power spectrum analysis was employed to identify the QBWO period and intensity and test their significances. Composite analysis approach was used to investigate the evolution and structure of the QBWO from 1991 to 2010. The details of this approach would be described in Section 4.

3 Variance distribution and power spectral analysis

3.1 Variance distribution

Kemball-Cook and Wang (2001) separated the boreal summer into the early stage (May–June, MJ) and the late stage (August–October, AO) since the boreal summer intraseasonal oscillation (BSISO) had quite different circulation systems during the two stages. They showed the seasonal variation of 10–100-day filtered OLR variance, and the maxima variance was concentrated in the Bay of Bengal, the Arabian Sea, and the eastern Indian Ocean during the MJ stage but shifted

to the South China (SCS) and Philippine Seas during the AO stage. However, the variance was strong in the Indian Ocean, as well as the South China and Philippine Seas in July. Thus, July was regarded as a transition between early and late summer and was excluded in their study. As an important component of BSISO, the QBWO is also presumed to have differences during the early and late summer. We chose May 1 to June 30 and August 1 to September 30 as the early and late summer, respectively, in this study.

Figure 1a, b exhibits the variance distribution of quasi-biweekly OLR and climatological atmospheric background from the early (MJ) and late (AS) summer. During the MJ stage (Fig. 1a), the significant variance is only concentrated over the SCS, accompanied by a weak cyclonic circulation (CC) to its west and an anticyclonic circulation (AC) to its east. The AC, reflecting the Western Pacific Subtropical High (WPSH), is strong to the east of Philippines during the MJ stage, unfavorable for convection development due to the suppression of the WPSH. However, the WPSH has a distinct northeastward displacement, and the enhanced CC extends eastward in July (not shown). The convection is active over most of the SCS, but with a little eastward spread to the northeast of Philippines, following the change of the WPSH. During the AS stage (Fig. 1b), the WPSH further retreats northeastward to the east of Japan, and the CC is also amplified as extending eastward. The convection is prevalent over both of the SCS and the northeast of Philippines, forming an elongated belt of large variance from the SCS through the western North Pacific along 20° N. Although the QBWO variance during the AS stage is greater than that during the MJ stage over the SCS, it is easily found that the region in the north of the SCS (17.5° N–22.5° N, 115° E–120° E indicated

by the boxes in Fig. 1a, b) is characterized by the maximum variance of QBWO during both two stages. Therefore, this region is chosen as the reference zone in this study.

The distributions of variance percentage (ratio of the 10–20-day variance to the total variance) during the MJ and AS stages are presented in subpanels c and d of Fig. 1, respectively. The variance percentage was distinct in the reference region in both stages, coinciding with the maximum variance over the SCS. It suggests the activities of QBWO in the reference region are prominent during the early summer and the late summer.

3.2 Power spectral analysis

To verify the significance of the QBWO signals over the SCS, power spectral analysis is conducted using daily OLR averaged within the reference region shown in Fig. 1. During the MJ stage (Fig. 2a), a peak can be found at a period of more than 15 days with 95 % confidence level. During the AS stage (Fig. 2b), there is a remarkable peak corresponding to the period of less than 15 days. It can be concluded that the 10–20-day convective signals are statistically significant during both stages. But two discernible differences in the power spectra between the two stages can be identified. One is that the peak QBWO period during the MJ stage seemed to be longer than that during the AS stage, which may be attributed to the discrepancies in QBWO origin and dominant triggering mechanism. The other is that the spectral power of QBWO during the MJ stage is weaker than that during the AS stage, which is consistent with the difference of variance magnitude during the two stages over the SCS mentioned earlier.

Fig. 1 Distributions of the variance of the 10−20 days OLR (*shaded*) and multiyear mean original wind at 850 hPa (*vector*) and its stream function (*contour*) for **a** May–June and **b** August–September of 1991–2010. Distributions of variance ratio of the 10−20 days to the total (*shaded*) for **c** May–June and **d** August–September of 1991–2010. Contour interval is 50 W^2 m^{-4} and 0.1×10^{-7} m^2 s^{-1} for OLR and stream function, respectively, in **a** and **b**, while it is 0.01 for the ratio in **c** and **d**. The area inside the *dashed line box* is the selected reference zone (17.5–22.5° N, 115–120° E)
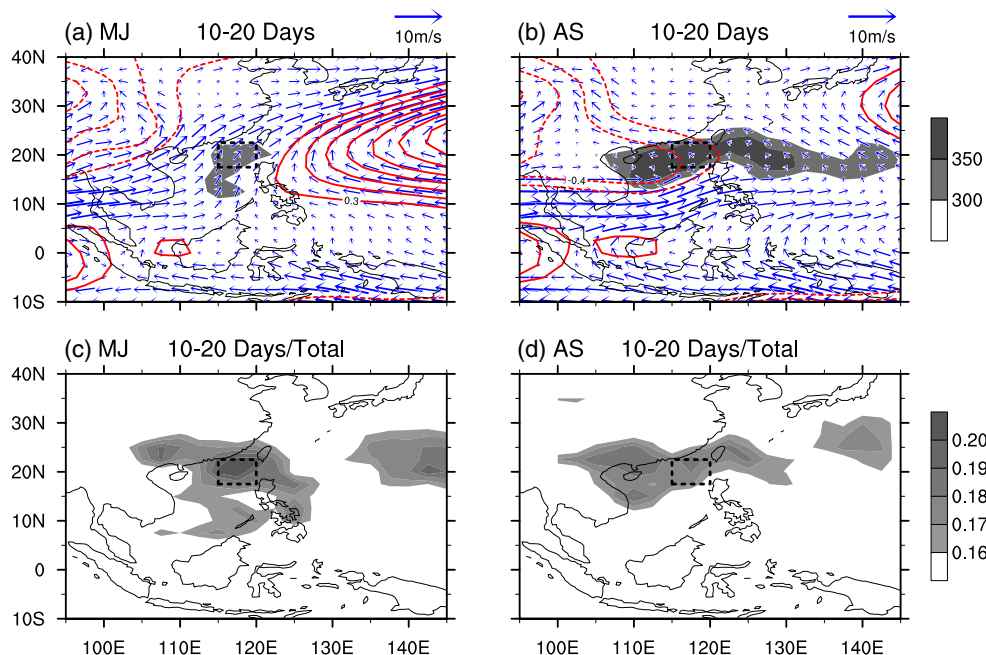
Fig. 2 Ensemble power spectra of OLR averaged over the SCS (17.5–22.5° N, 115–120° E) during **a** May–June and **b** August–September of 1991–2010. Red noise spectrum (*blue dashed line*) and the 95 % confidence level (*red solid line*) are also shown
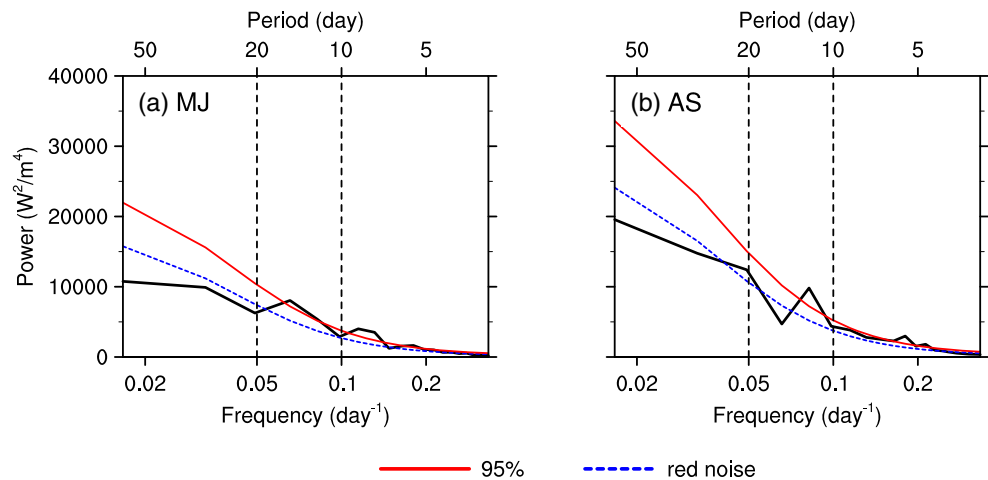
4 Evolutions of the QBWO during the two stages

4.1 Composite analysis

The evolutions of the QBWO in convection during the MJ and AS stages can be described by composites based on the filtered time series. A complete cycle of QBWO consists of lagged days from day −6 to day 6 (here, day 0 represents the day of the most active convection anomaly) for the two stages in this composite study (Fig. 3), similar to Fukutomi and
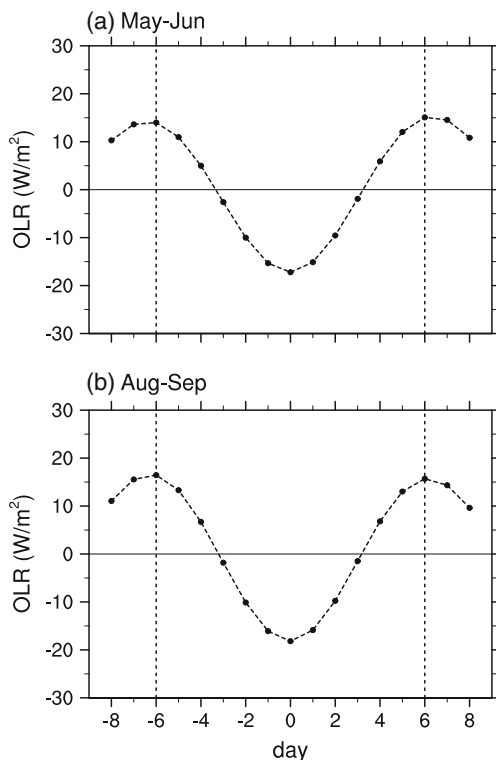
Fig. 3 The composite phases of 10–20-day OLR anomaly averaged over the SCS for **a** May–June and **b** August–September of 1991–2010

Yasunari (1999). A total of 30 and 36 cases are selected for the composites during the MJ and AS stages from 1991 to 2010, respectively. The criteria of case selection are as follows: (1) there is a complete and distinct phase cycle for the 10–20-day convection anomaly; (2) the minimum standardized OLR anomaly (day 0) in a cycle must be less than the negative one standard deviation, and (3) the previous and subsequent maximum positive OLR anomalies (day −6 and day 6) in a cycle must be larger than one standard deviation. The dates of the minimum OLR anomalies in individual cases are defined as the reference dates for the composites. The anomaly fields during the period from day −6 to day 6 for all cases are composited for each stage to investigate the evolutions of the QBWO. In this composite study, the statistical significance at 95 % level is conducted using the same method as that in Murakami (1987). Based on the null hypothesis that the two means for day $i-6$ and day i ($i=0$, 6) are equal, the ratio

$$t = \frac{\left(\overline{X}_i - \overline{X}_{i-6}\right)}{\left(\frac{S_i^2 + S_{i-6}^2}{N-1}\right)^{1/2}}, \tag{1}$$

is distributed as a t distribution. N is the number of cases (30 for the MJ stage and 36 for the AS stage). $\overline{X}_i$ and S_i^2 are the mean and variance for each day, respectively.

4.2 The evolutions of the QBWO

The successive composite maps of the 10–20-day OLR from day −6 to day 5 during the early (MJ) and late (AS) stages are presented in Figs. 4 and 5, respectively. Figure 4a–g presents the development process of the active QBWO over the SCS during the MJ stage. On day −6 (Fig. 4a), there is a clear positive OLR anomaly over the SCS. This positive anomaly gradually decays locally in the next few days and finally

Fig. 4 a–l Spatial distributions of composite 10–20-day OLR (*shaded*), 850-hPa wind (*vector*), and its stream function (*contour*) from day −6 to day 5 during the May–June stage. Intervals for OLR and stream function are 6 Wm^{-2} and 0.3×10^6 m^2 s^{-1}, respectively. Only locally statistically significant (>95 %) OLR and wind are shown
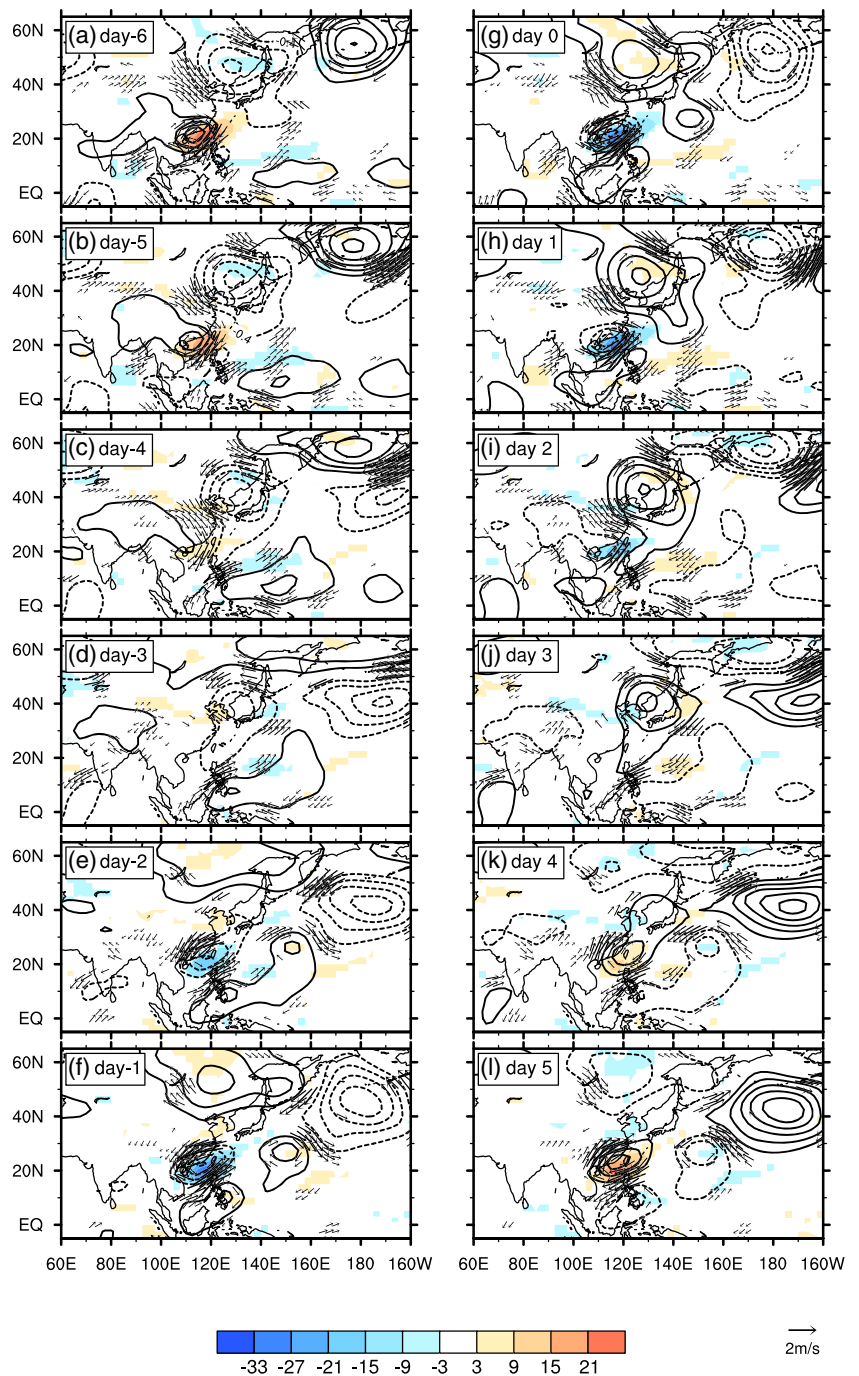
disappears on day −3 (Fig. 4d). Subsequently, on day −2 (Fig. 4e), a significant negative OLR anomaly emerges over the SCS. This negative anomaly develops and matures on day 0 (Fig. 4g). Figure 4g–l exhibits a mirror image with an opposite sign (Fig. 4a–f). The most active QBWO over the SCS decays gradually after day 0 and disappears on day 3 (Fig. 4j), but then, a positive OLR anomaly appears again over the SCS on day 4 (Fig. 4k) and develops locally. This local QBWO may be connected with the local air–sea interaction over the SCS. In addition, on day −4 (Fig. 4c), a weak negative OLR

anomaly appears to the east of Japan, and this anomaly begins to extend southwestward slowly on day −3 (Fig. 4d) and gradually connects with the emerged negative OLR anomaly over the SCS. A close connection between the anomalies from east of Japan and those over the SCS can be found on day −1 (Fig. 4f). Similar evolutions for the positive OLR anomaly over the east of Japan are presented from day 2 to day 5 (Fig. 4i–l). It implies that the rapid development of the local anomaly over the SCS on day −2 (Fig. 4e) is due to the facilitation of the anomaly from the east of Japan. Summing up,

Fig. 5 a–l Same as Fig. 4, except for August–September
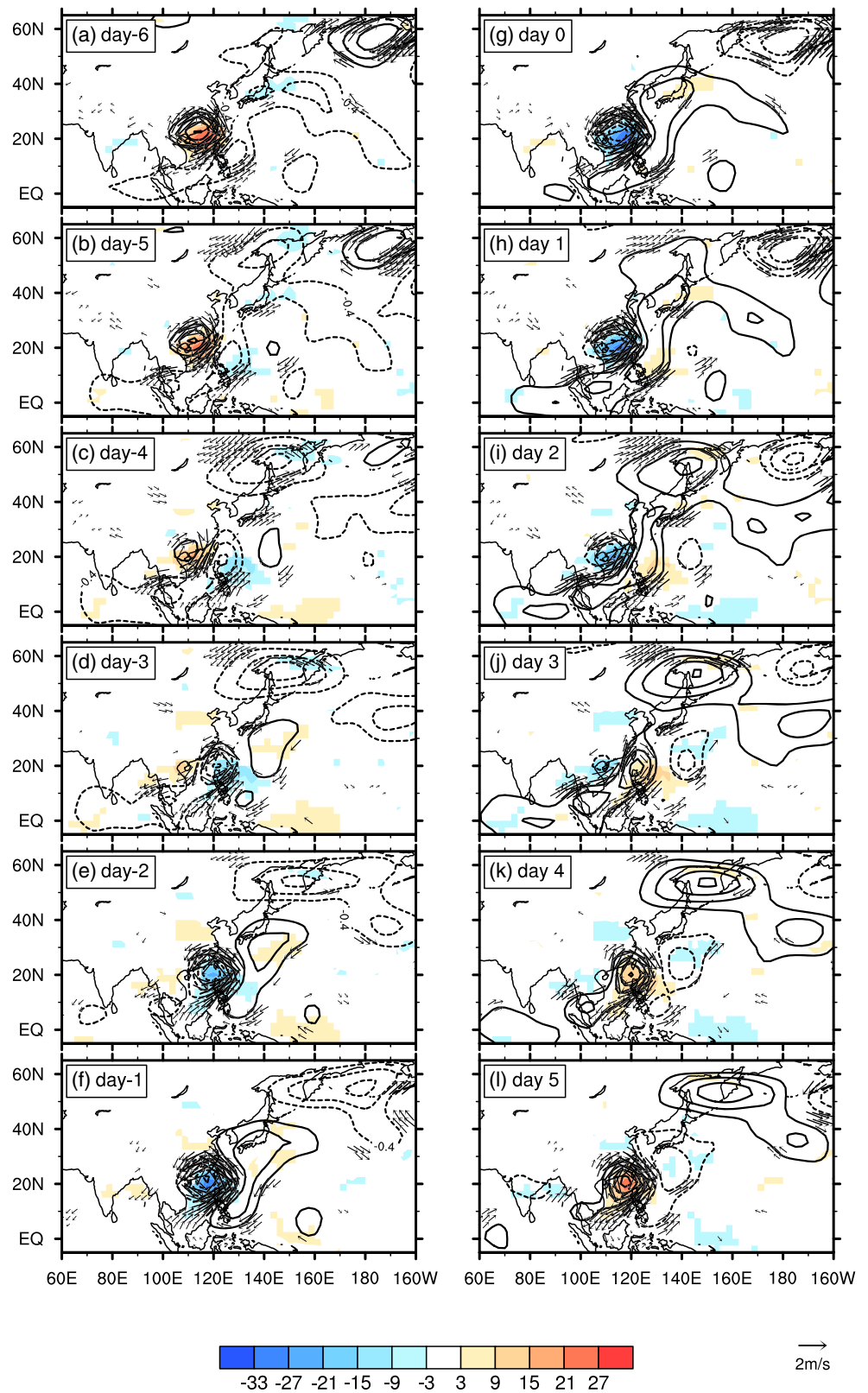
during the MJ stage, a local QBWO over the SCS exists, which could be strengthened by the southwestward extension of QBWO anomaly from the east of Japan.

Similarly, Fig. 5 presents a complete evolution of the QBWO over the SCS during the AS stage but with quite different features. On day −6 (Fig. 5a), there is a mature

positive OLR anomaly over the SCS. But this anomaly decays while propagating westward in the next few days and disappears over the continent of China, near 105° E on day −1 (Fig. 5f). Meanwhile, a weak negative OLR anomaly appears to the east of the Philippines on day −5 (Fig. 5b) and then develops northwestward. After it arrives at the south of Taiwan on day −2 (Fig. 5e), the OLR anomaly migrates westward and matures over the SCS on day 0 (Fig. 5g). Subsequently, the negative OLR anomaly decays similarly to the west and finally disappears over the continent of China from day 0 to day 5 (Fig. 5g–l). Meanwhile, a positive OLR anomaly emerges to the east of the Philippines on day 1 (Fig. 5h) and experiences similar evolutions in the following 4 days (Fig. 5h–l), just as the negative OLR anomaly does. In contrast to the dominant local character of the QBWO cycle over the SCS during the MJ stage, the QBWO during the AS stage mainly propagates in its life cycle.

4.3 The low-level circulations

The distributions of 850-hPa circulation anomalies associated with the QBWO during both stages are also presented in Figs. 4 and 5. During the MJ stage, the strong positive OLR anomaly over the SCS is accompanied by a distinct wave train of 850-hPa stream function extending from the SCS to the North Pacific (NP) on day −6 (Fig. 4a). This wave train consists of a cyclonic circulation over Northeast Asia (NEA) and two anticyclonic circulations over the SCS and NP, respectively. As the positive OLR anomaly decays locally with time, the circulation anomaly over the SCS also weakens gradually during the next few days (Fig. 4b–e). Meanwhile, the southeast part of the NEA cyclonic anomaly begins to penetrate southwestward from day −5 (Fig. 4b) and arrives over the SCS on day −2 (Fig. 4e) to replace the original anticyclonic circulation, accompanied by the negative OLR anomaly. This southwestward extension of the circulation precedes the southwestward propagation of the negative OLR anomaly from the east of Japan (Fig. 4c–e). Over the SCS, the negative OLR anomaly and the cyclonic circulation develop and both mature on day 0 (Fig. 4g). At that time, the significant negative OLR anomaly over the SCS is accompanied by a wave train of 850-hPa stream function with a negative–positive–negative pattern in a southwest–northeast orientation on day 0. The subsequent evolutions of the circulations from day 1 to day 5 (Fig. 4h–l) are similar to that from day −5 to day −1 but with opposite signs.

Unlike the wave train from the SCS to the NP during the MJ stage, a southeast–northwest wave train originated from the equatorial region emerges on day −6 during the AS stage (Fig. 5a). On day −5 (Fig. 5b), the wave train propagates northwestward, and the negative OLR anomaly appears southeast of the cyclonic circulation. In the next few days (Fig. 5c–f), this wave train

continues to propagate northwestward and finally terminates over the Southeast China. During this period, the negative OLR anomaly migrates from the east of the Philippines to the south of Taiwan following the wave train and then propagates toward the west. On day 0 (Fig. 5g), a visible northwestward positive–negative wave train of stream function appears from the tropics. Its subsequent evolutions (Fig. 5h–l) are also similar to that from day −5 to day −1 but with opposite signs.

4.4 The propagation characteristics

The propagation characteristics during the two stages are investigated to confirm the aforementioned evolution characteristics in Figs. 4 and 5. Figure 6a exhibits the cross sections to demonstrate the propagation characteristics of the QBWO during both stages. For the MJ stage, the cross section is from P0 (37.5° N, 150° E) to P1 (12.5° N, 102.5° E) (shown as the red dashed line in Fig. 6a). For the AS stage, two cross sections are selected, considering the change of propagation direction of OLR anomaly during the AS stage. One is from P2 (5° N, 140° E) to P3 (20° N, 120° E) (shown as the blue dashed line in Fig. 6a) and the other from P3 (20° N, 120° E) to P4 (20° N, 100° E) (shown as the green dashed line in Fig. 6a). In addition, several representative positions (the east of Japan and the SCS for the MJ stage and the east of the Philippines, the SCS, and the continent of China for the AS stage) are also labeled in Fig. 6a for reference.

Figure 6b presents the evolution characteristics of the QBWO along the cross section during the MJ stage. A distinct positive–negative–positive variation of the OLR anomaly with time is present over the SCS (20° N, 117.5° E), implying that the local oscillation is dominant during this stage. A weak negative OLR anomaly appeared to the east of Japan (35° N, 145° E) around day −4 and extended southwestward slowly with time, is connected with the SCS negative anomaly, and finally reaches its peak. Figure 6c presents the propagation characteristics of the QBWO along the two cross sections (AS1 and AS2) during the AS stage. It exhibits a significant northwestward propagation from the east of the Philippines (12° N, 130° E) to the south of Taiwan (P3) (20° N, 120° E), and then a westward migration to the SCS (20° N, 117.5° E), followed by the dissipation over the continent of China (20° N, 105° E). These results are consistent with the northwestward and then westward migration of QBWO described in Fig. 5. Different from the local oscillation over the SCS during the MJ stage, the QBWO during the AS stage features a more northwestward propagation from the east of the Philippines to the continent of China.

To sum up, the QBWO over the SCS is mainly characterized by a local oscillation during the early stage. In
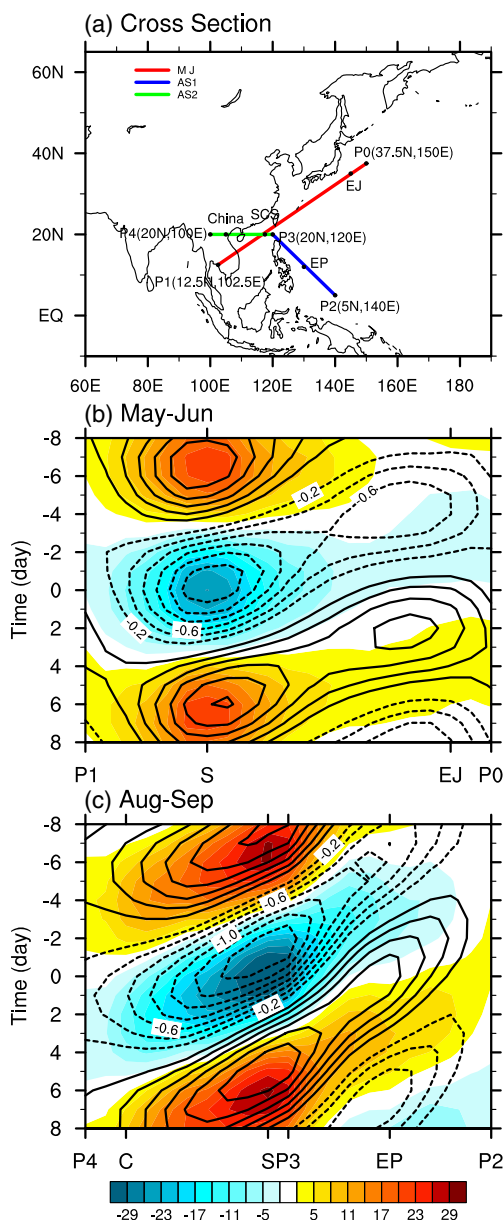
Fig. 6 **a** The cross sections during the two stages. The P0–P1 section is for the MJ stage (*red line*), the P2–P3 section for the first cross section during the AS stage (AS1, *blue line*), and the P3–P4 section for the second cross section during the AS stage (AS2, *green line*). The reference regions include the South China Sea (*S*), the east of Japan (*EJ*), the east of the Philippines (*EP*), and the continent of China (*C*). The propagation characteristics of QBWO along the selected cross sections during the **b** MJ and **c** AS stages, respectively. Contour intervals are 3 W^2 m^{-4} for OLR (*shaded*) and 0.2×10^6 m^2 s^{-1} for stream function (*contour*)

collaboration with the southwestward extension of QBWO anomaly from the east of Japan, the QBWO signal over the SCS is strengthened cooperatively. In contrast, the QBWO during the AS stage propagates northwestward from the east of the Philippines to the south of Taiwan and then shifts westward, matured over the SCS, and finally dissipates over the continent of China.
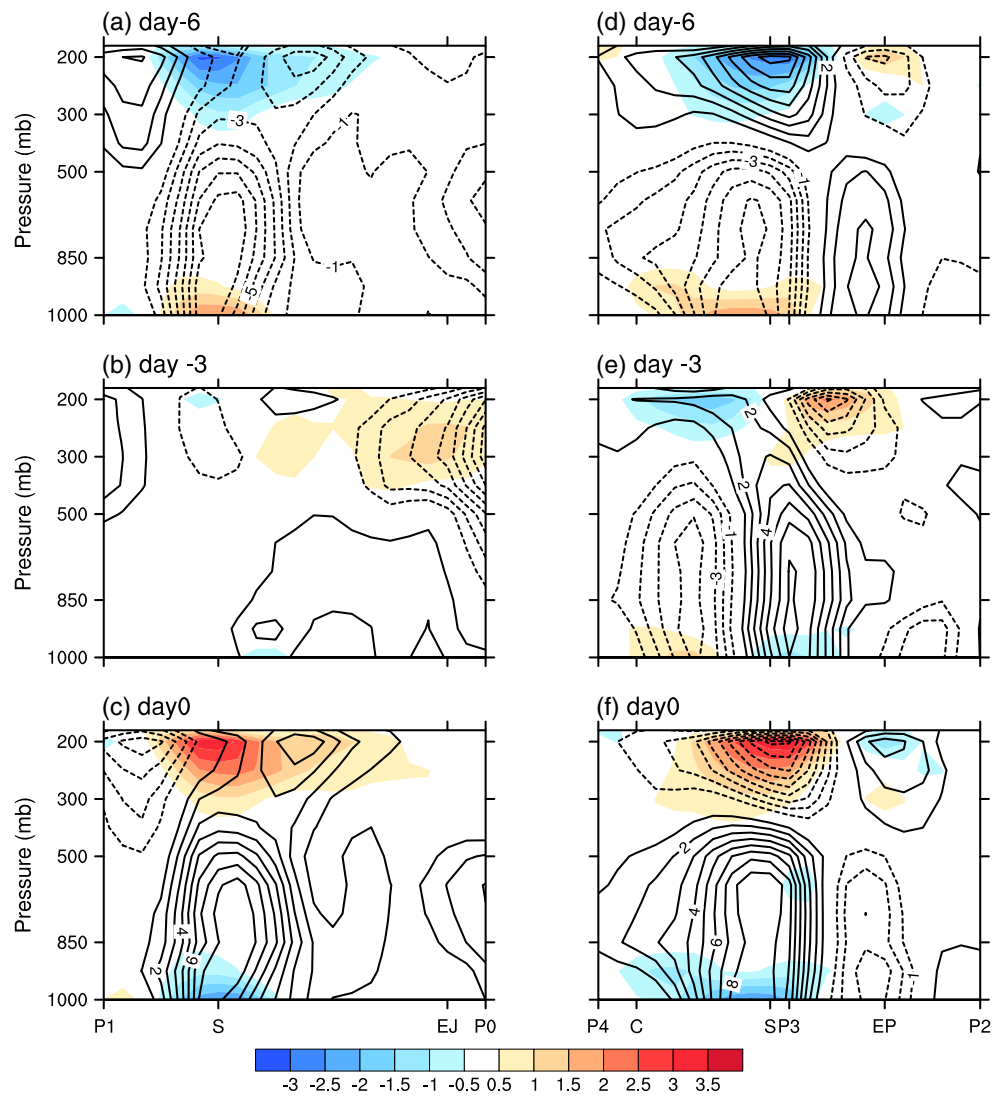
5 Vertical structures of the QBWO during the two stages

The vertical structures of the QBWO during both stages are shown in Figs. 7 and 8, in terms of relative vorticity, divergence, vertical velocity, and temperature fields. The left and right panels are for the MJ and AS stages, respectively. Overall, the active (inactive) convection corresponds to the low-level convergence (divergence) and upper-level divergence (convergence), as well as upward (downward) motion through the troposphere during both stages. However, detailed comparison sheds light on the noticeable differences between the two stages. Only the development period from day −6 to day 0 is discussed because the decaying period is simply with an opposite sign. Figure 7a displays that, during the MJ stage, a negative vorticity corresponding to the positive OLR anomaly over the SCS exhibits a northeast tilt with height on day −6, and the low-level divergence and upper-level convergence match well to the maximum OLR anomaly. In the following days, the negative vorticity anomaly over the SCS diminishes, and a low-level positive vorticity (below 500 hPa) from southwest of the east of Japan (EJ) expands and penetrates southwestward gradually (not shown). On day −3 (Fig. 7b), the previous negative vorticity over the SCS disappears, whereas the low-level positive vorticity from the northeast reaches the SCS. The divergence is obscure at this positive-to-negative transition time of OLR. On day 0 (Fig. 7c), the relative vorticity and divergence transform locally into their opposite patterns. In collaboration with the positive vorticity from the northeast, a robust and vertically extending positive vorticity anomaly forms over the SCS and tilts northeastward with height.

During the AS stage, the wave trains with alternating positive–negative relative vorticity and divergence are pronounced at both low and upper levels in the cross sections on day −6 (Fig. 7d). Similar to the MJ stage, a negative vorticity corresponds to the positive OLR anomaly over the SCS. Instead of a northeast tilt with height, the negative vorticity extends up to near 300 hPa, while a positive vorticity appears above. In the following days, the wave train propagates northwestward and then westward with gradually decaying toward the west of the SCS (not shown). On day −3 (Fig. 7e), the positive vorticity from EP already arrives in the south of Taiwan (P3), and the previous negative vorticity in the P3–P4 section leaves the SCS region and decays to the west. On day 0 (Fig. 7f), a wave train with opposite phase appears over the SCS in the cross section, which is characterized by a positive vorticity extending up to near 300 hPa and a negative vorticity above. In addition, during the entire evolution process, the lower-level convergence (divergence) and upper-level divergence

Fig. 7 Vertical structures of the relative vorticity (*contour*) and divergence (*shaded*) on days −6, −3, and 0 during the **a–c** MJ and **d–f** AS stages. Intervals for relative vorticity and divergence are 1.0×10^6 and $0.5 \times 10^6 \ s^{-1}$, respectively


(convergence) migrate along with the positive (negative) vorticity anomaly.

The vertical structures of air temperature during the two stages are shown in Fig. 8. During the MJ stage, a large region with warm anomaly appears to the northeast of the SCS, while a weak cold anomaly exists to the southwest of the SCS between 200 and 500 hPa on day −6 (Fig. 8a). This suggests that the QBWO featured over the SCS during the MJ is susceptible to the influences of midlatitude systems. The positive OLR anomaly over the SCS is accompanied by a low-level warming and an upper-level cooling. However, on day −3 (Fig. 8b), the temperature structure is obscured over the SCS, but on day 0 (Fig. 8c), it exhibits an opposite temperature pattern. During the AS stage, a distinct cold anomaly center is present between 200 and 500 hPa over the SCS on day −6 (Fig. 8d), with a weaker warm anomaly beneath. On day −3 (Fig. 8e), a warm center at about 250 hPa emerges to the south of Taiwan (P3). On day 0

(Fig. 8f), a significant warm anomaly between 200 and 500 hPa exists over the SCS, while a weaker cold anomaly appears beneath (at ~850 hPa).

The comparison shows that vertical structures during both stages have the similar temperature anomalies but with different magnitudes. The vigorous negative (positive) temperature anomaly exists at the lower (upper) level during the MJ (AS) stage. In addition, the cold anomaly at the low level on day 0 (Fig. 8c, f) may be ascribed to the reduction in sensible or latent heat flux from the cold ocean due to the decreased solar shortwave radiation which results from the large fraction of cloud coverage corresponding to increased convection. Besides, the precipitation in the stage of active convection can also generate evaporative or melting cooling below the cloud layer. On the other hand, the warm anomaly at the upper level on day 0 (Fig. 8c, f) might be associated with the moisture uplift with upward motion due to the active 10–20-day convection, which

Fig. 8 Same as Fig. 7, except for the vertical structures of vertical velocity (*contour*) and air temperature (*shaded*). Intervals for vertical velocity and temperature are 0.005 Pa s^{-1} and 0.1 K, respectively
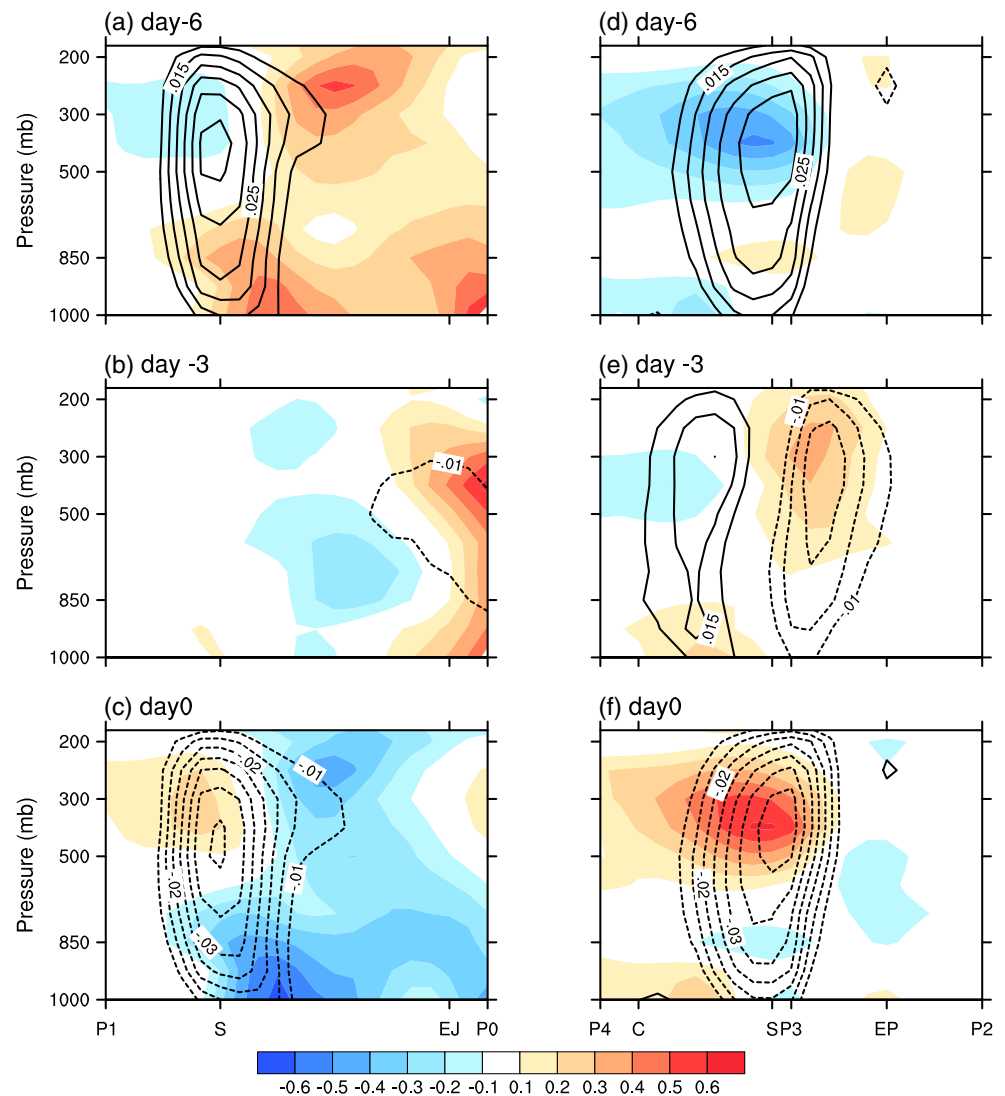
can release the heat of condensation and thus warm the surrounding air at the upper level. However, factors controlling the discrepancy in the magnitude of temperature anomaly remain unclear.

6 Preliminary analysis and discussion

6.1 Preliminary analysis

In this section, we carry out preliminary analyses and discussion to interpret the different characteristics of the QBWO activity during the MJ and AS stages. It is well known that the WPSH is an important circulation system during summer, and it can significantly suppress the development of multiscale convection due to the large-scale descending motion related to the WPSH. Because the WPSH intensity and coverage vary in different summer stages, the WPSH is considered to have different influences on the QBWO activities in

convection during the two stages. Figure 9 shows the coverage of the WPSH represented by the geopotential height of 5, 880 gpm at 500 hPa during the early and late stages. During the MJ stage (Fig. 9a), the WPSH is mainly situated to the east of Philippines, and its ridge line is oriented approximately along 20° N, farther away from the region to the east of Japan where convection is not suppressed. That may be favorable for the southwestward extension of the QBWO from the east of Japan along the western edge of the WPSH, which helps to strengthen the convection over the SCS during the MJ stage. Comparatively, the convective anomalies to the east of the Philippines can be directly suppressed by the WPSH. Thus, the convection tends to be inactive in this region, which is attributable to the inactive QBWO to the east of the Philippines.

In contrast, during the AS stage (Fig. 9b), the WPSH is enhanced and shifted northeastward, and its ridge line is displaced along 30° N. Correspondingly, the convection to the east of Japan is diminished by the WPSH during this stage.

(a) May-Jun

(b) Aug-Sep
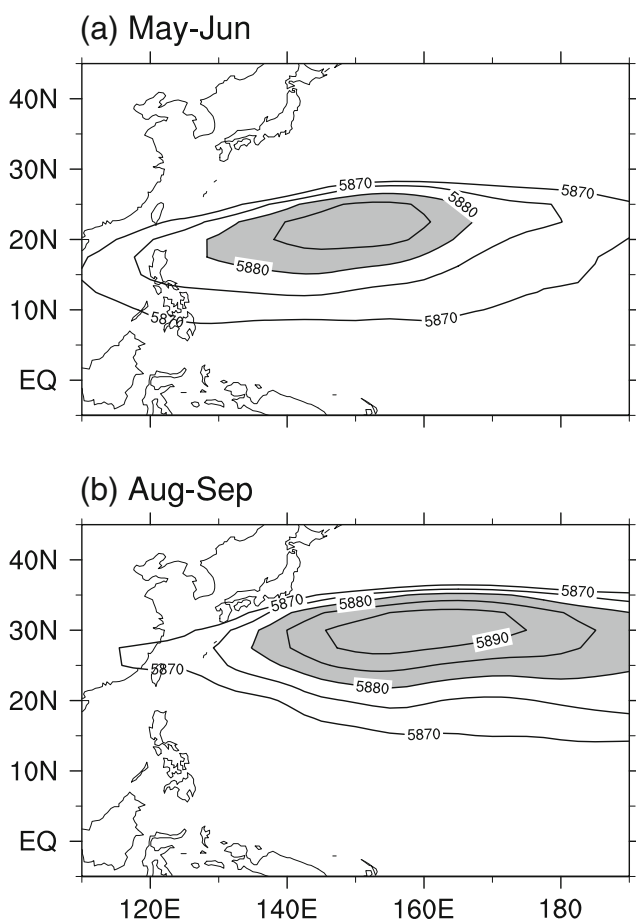
Fig. 9 Distributions of multiyear mean geopotential height at 500 hPa (*contour*) during **a** May–June and **b** August–September of 1991–2010. The areas greater than 5,880 gpm are *shaded*, representing the Western Pacific Subtropical High (WPSH)

On the contrary, the tropical region to the east of Philippines is distant from the WPSH, and thus, the convection in this region becomes more active. In general, the intensity and coverage of the WPSH may play crucial roles in modulating the occurrence and characteristics of the convection and further impact the evolution and propagation of the QBWO over the SCS. Yang et al. (2014) found the differences of quasi-biweekly characteristics over EA at early (June 10–July 20) and late (July 21–August 31) summer. They considered the abrupt changes of mean state in mid to late July, which includes the northward migration of westerly jet, South Asia High (SAH) and WPSH, and the weakening and broken of westerly jet, are the root causes of the change in behavior of quasi-biweekly variability (QBV). Yang et al. (2014) also indicated that the tropical monsoon trough and midlatitude westerly jet were the possible sources of QBV over subtropical EA in both subseasons and were useful to provide guidance for 2–3-week predictions over the EA. In our study, we have conducted preliminary analysis on how the WPSH influence the QBWO during summer. We also suppose that the seasonal

northward march of WPSH is one of the important elements for the subseasonal differences, just as shown in Fig. 9.

6.2 Discussion

For the QBWO over the SCS during the MJ shown in Section 5, a local oscillation dominates. It is hypothesized that the air–sea interaction over the SCS is responsible for this local feature. The positive OLR anomaly over the SCS on day −6 is indicative of reduced convection and cloud coverage, leading to an enhancement of solar shortwave radiation. As a result, the sea surface temperature anomaly (SSTA) increases locally due to the absorption of solar radiative heating. Subsequently, the warm SSTA would exert feedback on the lower-level atmosphere by triggering convective instability, causing the initiation of convection and thus the negative OLR anomaly. Then, the enhanced convection would decrease the solar radiative heating and then generates negative feedback to the SSTA. The detailed analysis is the subject of an ongoing work and will be reported in the future.

Regarding the southwestward extension of the convection anomalies from the east of Japan during the MJ stage, the mechanism is still unclear. Fukutomi and Yasunari (1999) described a similar pattern, in which the 10–25-day convection anomalies over the SCS were associated with large-scale circulation in the Asian-Pacific region for four early summer seasons from 1991 to 1994 (the early summer was defined as June to July for 1991, 1992, and 1994 but as June to August for 1993). There was a southwest–northeast-oriented wave train extending from the SCS to the North Pacific in the lower troposphere. The anomalous anticyclone moved southwestward from the subtropics into the SCS along the wave train and caused suppressed convection subsequently. Following the inactive convection over the SCS, the southwestward-propagating subtropical cyclonic anomalies triggered the subsequent active convection in the SCS. From this study, we can see that the wave train connected the convection anomalies over the SCS with those in the subtropics, as a Rossby mode response to the anomalous heating (cooling). The southwestward extension of the 10–20-day convection anomalies from the east of Japan to the SCS in this study also bears some resemblances to that described in Fukutomi and Yasunari (1999).

The northwestward propagation of the anomalies from the tropics to the south of Taiwan during the AS stage is similar to the results in Chen and Sui (2010). In their study, the QBWO presented by 10–20-day vorticity emerged from the equatorial region and propagated northwestward along an alternating cyclonic and anticyclonic wave train with a southeast–northwest orientation and a wavelength of about 3,500 km. The energetic analysis in their study revealed that the waves were maintained through baroclinic conversion in the subtropics

(north of 25° N) and diabatic latent heating in the tropics. The diabatic heating in the tropics and baroclinic conversion in the subtropics were jointly converted to the eddy available potential energy (EAPE) and then further converted to the eddy kinetic energy (EKE). The EKE produced by conversion from the EAPE and barotropic processes would be redistributed by the convergence of eddy geopotential flux and advection by mean and perturbation winds. This underlying mechanism for the QBWO development and maintenance may be useful to explain the propagation characteristic during the AS stage in this study.

7 Summary

In this study, different characteristics of QBWO over SCS during the MJ and AS stages are investigated. The composite results show the main discrepancies as follows.

First, the intensity and peak period of the QBWO over SCS differ in the two stages. Power spectral analysis reveals that the QBWO has a smaller power spectrum and longer period during the MJ stage in comparison with that during the AS stage.

Second, the origin and characteristics of the QBWO are quite different during the two stages. During the MJ stage, the QBWO over the SCS is mainly characterized by a local oscillation, which is strengthened in conjunction with the southwestward extension of QBWO anomaly from the east of Japan. During the AS stage, the QBWO signal originates from the southeast of Philippines. The QBWO anomaly in the equatorial region moves northeastward to the south of Taiwan and then shifts toward the west, peaks over the SCS, and then decays toward the west.

A wave train of low-level circulation persists from the SCS to the NP during the MJ stage, whereas it origins from the equator during the AS stage. The vertical structures of the QBWO during both stages are revealed. In general, the active (inactive) convective anomaly is accompanied by a convergence (divergence) at the low level, a divergence (convergence) at the upper level, and an ascending (descending) motion through the deep troposphere. On the other hand, the significant differences in vertical structures of relative vorticity and air temperature could be observed during the two stages. On day 0, the positive vorticity anomaly over the SCS exhibits a northeast tilt with height during the MJ stage, while it extends up to near 300 hPa with a negative vorticity anomaly above during the AS stage. There is the southwestward extension of the vorticity from the east of Japan to the SCS during the MJ stage, but there exists a northwestward propagation of wave-like vorticity anomaly during the AS stage. Moreover, the temperature anomaly is significant at the low level during the MJ stage but is pronounced at the upper level during the AS stage.

Finally, a preliminary analysis is carried out to interpret the differences of QBWO based on the distributions of the WPSH during the two stages. It is found that the QBWO origin and propagation over the SCS may be associated with the migration of the WPSH. During the MJ stage, the development of convection anomalies to the east of Japan avoids the unfavorable environment, thanks to being farther away from the WPSH. But during the AS stage, the QBWO signal originates from the southeast of the Philippines without the suppression associated with the WPSH, which shifts northward and retreats eastward. It suggests that the WPSH may play a crucial role in modulating the origin and characteristics of the QBWO over the SCS during boreal summer. Moreover, the relevant discussion on the findings in previous studies is presented to provide the basic guidance for further investigations.

References

Chan JC, Ai W, Xu J (2002) Mechanisms responsible for the maintenance of the 1998 South China Sea summer monsoon. J Meteorol Soc Jpn 80:1103–1113

Chen G, Sui CH (2010) Characteristics and origin of quasi-biweekly oscillation over the western North Pacific during boreal summer. J Geophys Res Atmos 1984–2012:115

Chen T-C, Chen J-M (1993) The 10-20-day mode of the 1979 Indian monsoon: its relation with the time variation of monsoon rainfall. Mon Weather Rev 121:2465–2482

Chen T-C, Yen M-C, Weng S-P (2000) Interaction between the summer monsoons in East Asia and the South China Sea: intraseasonal monsoon modes. J Atmos Sci 57:1373–1392

Duchon CE (1979) Lanczos filtering in one and two dimensions. J Appl Meteorol 18:1016–1022

Fukutomi Y, Yasunari T (1999) 10–25 day intraseasonal variations of convection and circulation over East Asia and western North Pacific during early summer. J Meteorol Soc Jpn Ser II 77:753–769

Goswami BN, RS Ajayamohan, PK Xavier, D Sengupta (2003) Clustering of synoptic activity by Indian summer monsoon intraseasonal oscillations. Geophys Res Lett 30, n/a-n/a.

Kalnay E et al (1996) The NCEP/NCAR 40-year reanalysis project. Bull Am Meteorol Soc 77:437–471

Kemball-Cook S, Wang B (2001) Equatorial waves and air–sea interaction in the boreal summer intraseasonal oscillation. J Clim, 14

Keshavamurty RN (1971) Power spectra of large-scale disturbances of Indian summer monsoon. Bull Am Meteorol Soc 52:796

Keshavamurty RN (1972) On the vertical tilt of monsoon disturbances. J Atmos Sci 29:993–995

Kikuchi K, Wang B (2009) Global perspective of the quasi-biweekly oscillation. J Clim 22:1340–1359

Kiladis GN, Wheeler M (1995) Horizontal and vertical structure of observed tropospheric equatorial Rossby waves. J Geophys Res Atmos 100:22981–22997, **1984–2012**

Krishnamurti T, Ardanuy P (1980) The 10 to 20-day westward propagating mode and "breaks in the monsoons". Tellus 32:15–26

Krishnamurti TN, Bhalme H (1976) Oscillations of a monsoon system. Part I. Observational aspects. J Atmos Sci 33:1937–1954

Li C, Jia X, Ling J, Zhou W, Zhang C (2009) Sensitivity of MJO simulations to diabatic heating profiles. Clim Dyn 32:167–187

Li RY, Zhou W (2014) Multiscale control of summertime persistent heavy precipitation events over South China in association with synoptic, intraseasonal, and low-frequency background. Clim Dyn, 1–15

Liang J, Wu L, Ge X, Wu C-C (2011) Monsoonal influence on typhoon Morakot (2009). Part II: numerical study. J Atmos Sci 68:2222–2235

Liebmann B (1996) Description of a complete (interpolated) outgoing longwave radiation dataset. Bull Am Meteorol Soc 77:1275–1277

Ling J, Li C, Zhou W, Jia X (2014) To begin or not to begin? A case study on the MJO initiation problem. Theor Appl Climatol 115:231–241

Liu H-B, Yang J, Zhang D-L, Wang B (2014) Roles of synoptic to quasi-biweekly disturbances in generating the summer 2003 heavy rainfall in East China. Mon Weather Rev, 142

Madden RA, Julian PR (1971) Detection of a 40–50 day oscillation in the zonal wind in the tropical Pacific. J Atmos Sci 28:702–708

Madden RA, Julian PR (1972) Description of global-scale circulation cells in the tropics with a 40–50 day period. J Atmos Sci 29:1109–1123

Mao J, Chan JCL (2005) Intraseasonal variability of the South China Sea summer monsoon. J Clim 18:2388–2402

Murakami T (1976) Cloudiness fluctuations during the summer monsoon. J Meteorol Soc Jpn Ser II 54:175–181

Murakami T (1987) Intraseasonal atmospheric teleconnection patterns during the northern hemisphere summer. Mon Weather Rev 115:2133–2154

Murakami T, Frydrych M (1974) On the preferred period of upper wind fluctuations during the summer monsoon. J Atmos Sci 31:1549–1555

Numaguti A (1995) Characteristics of 4-to-20-day-period disturbances observed in the equatorial Pacific during the TOGA COARE IOP. J Meteorol Soc Jpn Ser II 73:353–377

Wang B, Liu J, Yang J, Zhou T, Wu Z (2009) Distinct principal modes of early and late summer rainfall anomalies in East Asia. J Clim 22:3864–3875

Wu L, Liang J, Wu C-C (2011) Monsoonal influence on typhoon Morakot (2009). Part I: observational analysis. J Atmos Sci 68:2208–2221

Yang J, Wang B, Bao Q (2010) Biweekly and 21–30-day variations of the subtropical summer monsoon rainfall over the lower reach of the Yangtze River basin. J Clim, 23

Yang J, Bao Q, Wang B, Gong D-Y, He H, Gao M-N (2014) Distinct quasi-biweekly features of the subtropical East Asian monsoon during early and late summers. Clim Dyn 42:1469–1486

Yasunari T (1981) Structure of an Indian summer monsoon system with around 40-day period. J Meteorol Soc Jpn 59:336–354

Zangvil A (1975) Upper tropospheric waves in the tropics and their association with clouds in the wavenumber-frequency domain

Zhou S, AJ Miller (2005) The interaction of the Madden-Julian oscillation and the Arctic Oscillation. J Clim. 18